Short range order in bimetallic nanoalloys: An extended X-ray absorption fine structure study

Anatoly I. Frenkel, Qi Wang, Sergio I. Sanchez, Matthew W. Small, and Ralph G. Nuzzo

Citation: J. Chem. Phys. **138**, 064202 (2013); doi: 10.1063/1.4790509
View online: http://dx.doi.org/10.1063/1.4790509
View Table of Contents: http://jcp.aip.org/resource/1/JCPSA6/v138/i6
Published by the American Institute of Physics.

Short range order in bimetallic nanoalloys: An extended X-ray absorption fine structure study

Anatoly I. Frenkel,[1,a)] Qi Wang,[1] Sergio I. Sanchez,[2] Matthew W. Small,[2] and Ralph G. Nuzzo[2,a)]
[1]*Department of Physics, Yeshiva University, 245 Lexington Avenue, New York, New York 10016, USA*
[2]*Department of Chemistry and the Frederick Seitz Materials Research Laboratory, University of Illinois in Urbana-Champaign, Urbana, Illinois 61801, USA*

(Received 26 November 2012; accepted 23 January 2013; published online 12 February 2013)

Partial coordination numbers measured by extended X-ray absorption fine structure (EXAFS) spectroscopy have been used for decades to resolve between different compositional motifs in bulk and nanoscale bimetallic alloys. Due to the ensemble-averaging nature of EXAFS, the values of the coordination numbers in nanoparticles cannot be simply interpreted in terms of the degree of alloying or segregation if the compositional distribution is broad. We demonstrate that a Cowley short range order parameter is an objective measure of either the segregation tendency (e.g., a core-shell type) or the degree of randomness (in homogeneous nanoalloys). This criterion can be used even in the case when the clusters are random but have broad compositional distributions. All cases are illustrated using the analyses of EXAFS data obtained in three different nanoscale bimetallic systems: Pt(core)-Pd(shell), Pd(core)-Pt(shell), and Pt-Pd random alloy. © *2013 American Institute of Physics*. [http://dx.doi.org/10.1063/1.4790509]

I. INTRODUCTION

Bimetallic nanoparticles (NPs) have attracted enormous attention because of their applications in catalysis, electrochemistry, and environmental science.[1–6] These particles may adopt a broad range of sizes (between 1 and 100 nm), shapes (e.g., polyhedral, spherical, nanorods, and tripods), crystal structures, compositions and exhibit various types of compositional ordering (e.g., random, intermetallic, core-shell, or cluster-on-a-cluser configurations).[7] The successful creation of such a wide variety of structural and compositional motifs has stimulated further development of new synthetic approaches focused on tailoring NP architectures to exhibit desired properties.[2,8–11] It has been shown previously, both experimentally[4] and theoretically,[6,12–15] that catalytic properties can be directly affected by the details of the nanoparticle: size, composition, uniformity, structure, shape, surface morphology, and ability to undergo reaction-driven restructuring. One of the main challenges towards the goal of rational synthesis of functional bimetallic nanoparticles is their precise, atomistic characterization during their "work," e.g., while facilitating catalytic reactions. Under such conditions, direct imaging and scattering methods either become unavailable or relatively inaccurate, especially in the size range of a few nanometers.

Among the many techniques available, extended X-ray absorption fine structure (EXAFS) is one of the preferred methods for investigating the geometric and compositional habits of bimetallic nanocatalysts due to its local structure sensitivity and excellent spatial resolution. Its ability to measure compositional habits of bimetallic NPs is due to the elemental specificity of the technique. The latter allows EXAFS to separately analyze the local environment of different elements in the NP. For example, in a bimetallic cluster comprised of elements A and B, EXAFS can look at the A_xB_{1-x} alloy and obtain their partial coordination numbers (CNs): N_{AA}, N_{AB}, N_{BA}, and N_{BB}. The total coordination numbers around each element and its first nearest metal neighbors (N_{AM} and N_{BM}) are the sum of their respective partial CNs. By comparing the values of N_{AM} and N_{BM} one can identify the species that have smaller total coordination number and are likely to segregate to the surface of the particle, while the other species then segregates to the core. For example, if $N_{AM} < N_{BM}$, then the atoms of type A are likely to be predominantly found within the surface layers, while the B atoms will favor occupancy of the core region. Most researchers have been exploiting this difference between the coordination numbers to examine the structural and compositional habits of nanoparticles.[16–18]

There is one problem that remains unexplored and poorly understood: the effect of ensemble averaging on the EXAFS analysis results. If the clusters are identical, the EXAFS results can be interpreted in terms of the geometric characteristics of such clusters. However, if the composition varies from cluster to cluster (including the case where the clusters segregate into A-rich and B-rich structures) the atomic arrangements predicted assuming each cluster in the ensemble can be viewed as an equivalent "representative cluster" becomes meaningless. Furthermore, as we show in this article, a sample with a broad inter-cluster compositional distribution but random intra-cluster distribution will appear nonrandom to EXAFS, signalling a core-shell motif, even if all individual clusters are perfectly random. We demonstrate how this and other inhomogeneities influence the predictions made using

a)Authors to whom correspondence should be addressed. Electronic addresses: Anatoly.Frenkel@yu.edu and r-nuzzo@illinois.edu.

EXAFS analysis by examining three test systems specially chosen for this purpose.

II. COWLEY SHORT RANGE ORDER PARAMETER

As mentioned in the Introduction, interpreting the coordination numbers in heterogeneous systems in terms of a "representative cluster" can be misleading. We will discuss two commonly encountered systems that require particular care. One example is when two different NP systems differ in homogeneity of their atomic distributions, and the other – in the degree of their randomness.

First, we consider a homogeneous system where all atoms have similar local environments within each NP. Two cartoons depicting two dimensional "nanoparticles" with this type of structure are shown in Figs. 1(a) and 1(b). Although the lattices are differently ordered, both types of atoms contain a similar number of neighbors for each element throughout the "cluster." The similarity becomes nearly perfect when the surface to volume ratio becomes negligible, i.e., for particles larger than 4–5 nm in diameter. Such atomic arrangements are homogeneous, as there is an equal probability to find any given atom type (A or B) anywhere within the NP. An example showing the other extreme is presented in the two cartoons in Fig. 1(d) where the atoms of each type (A or B) are segregated within different part of the NP.

The second case we briefly discuss is when the two NP systems differ in the randomness of their atomic distributions. This characteristic will only apply to the homogeneous systems such as two NPs shown in Figs. 1(a) and 1(b), because the two NPs shown in Figs. 1(c) and 1(d) are heterogeneous, i.e., inherently nonrandom. The cluster in Fig. 1(a) has perfect order: both atomic types have equivalent surroundings. The cluster in Fig. 1(b) is random: for either atom (of type A or B), the probabilities of neighboring atoms being either type A or B are equal. One important consequence apparent from this simple example is the difference between the short range order and homogeneity. For example, an alloy can be homogeneous but have a "negative tendency to clustering" (i.e., short range order) and is a phenomenon frequently encountered in metallurgy.[19,20]

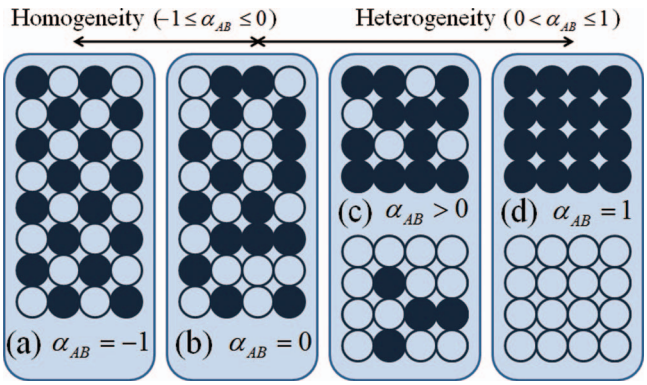

FIG. 1. Examples of homogeneous and heterogeneous packing of atoms in a two-dimensional lattice with 50-50 composition. Schemes (a) and (b) illustrate that a range of homogeneous configurations for the same composition is possible, all characterized by a unique, non-positive value of the short range order parameter α. Different heterogeneous configurations, all characterized by positive values of α, are shown in schemes (c) and (d).

These two examples illustrate the importance of understanding the short range order and homogeneity of bimetallic NPs when attempting to characterize their structure. It turns out that both of these can be quantitatively expressed using J. Cowley's short range order parameter:[21–23]

$$\alpha = 1 - \frac{N_{AB}/N_{AM}}{x_B}, \tag{1}$$

where x_B is the molar concentration of B-type atoms in the sample. As we will show below, the Cowley parameter (α can vary in the interval between -1 and 1) can be used to investigate the degree of alloying or clustering within bimetallic nanoparticles based on how positive/negative it is. In many cases, it can be used also as a "litmus test" demonstrating that atomic segregation, of either intra-cluster or inter-cluster type, occurred. We note that this equation has been previously employed in EXAFS studies of bulk bimetallic alloys[24] but its potential in nanoparticle studies remains unexplored.

For alloys that favor (disfavor) clustering of like atoms, α will be positive (negative). This parameter is therefore essential for studies of alloy – or core-shell, or cluster-on-cluster – NPs that can be characterized by different levels of ordering. Only after the short range order parameter is evaluated, can different models of segregation be compared. In either case, additional experimental information is needed to determine the fine detail of segregation, i.e., whether, e.g., element A is predominantly at the surface or in the core. The analogue of the effect of compositional heterogeneity on the interpretation of the short range order within a "representative" NP is the interpretation of the size of the "representative" NP from EXAFS coordination numbers. In each case, an independent technique is needed, and in the latter case, the average particle size can be measured by electron microscopy.

We emphasize that the role of measuring and evaluating α extends beyond merely determining whether it is positive or negative. Even large negative values of α may signal segregation as there is only a finite range $\alpha_{\min} \le \alpha \le 0$ in which homogeneous systems can exist.[21] For example, $\alpha_{\min} = -1$ for two dimensional AB alloys shown in Fig. 1(a), for β-brass CuZn of bcc structure,[21] but it can also be fractional, e.g., $\alpha_{\min} = -1/3$ for fcc $Cu_{0.75}Au_{0.25}$ alloys.[21] Hence, if the measured value of α falls within either $-1 \le \alpha \le \alpha_{\min}$ or $0 < \alpha \le 1$ interval, the system is heterogeneous and the segregation of atoms is evident. Finally, we note that these conclusions were obtained assuming an idealized case where all particles are equivalent and the segregation may occur only within the NP. If the bimetallic composition varies from one NP to another, even random compositional distribution may generate positive values of α, a point which is discussed in greater detail below.

III. EXPERIMENT, DATA PROCESSING AND ANALYSIS

To test EXAFS analysis methods based on the interpretation of the short range order parameters we chose the following three bimetallic nanoparticle samples of similar average size but different compositional distributions: (1) Pt in the

core and Pd in the shell (Pt@Pd), (2) Pd in the core and Pt in the shell (Pd@Pt), and (3) random Pt-Pd nanoalloys. These systems have been studied previously by aberration corrected transmission electron microscopy.[25] To synthesize the core-shell particles, monometallic Pd and Pt NPs were prepared first, via a polyol method[26] using polyvinylpyrrolidone (PVP, MW = 40 000 g/mol) and degassed ethylene glycol. Both types of core-shell Pt-Pd (50:50) NPs were synthesized using the "sacrificial hydrogen layer" method developed by Toshima *et al.*[27] Following this method, premade monometallic Pd (or Pt) NPs dispersed in ethanol were coated with hydrogen and then exposed to the secondary metal ions (either Pt^{2+} or Pd^{2+}) at room temperature. Random alloy Pt-Pd (50:50) NPs were synthesized by a co-reduction of H_2PtCl_6 and $PdCl_2$ refluxed in degassed ethylene glycol in the presence of PVP. More details of the NP's preparation procedures can be found in Ref. 25. TEM studies show that as synthesized NPs are spherical in shape and with size distributions centered at about 2.4(4) nm for the monometallic and random alloy NPs, and at about 3.5(5) nm for the core-shell NPs. Energy dispersive X-ray spectroscopy (EDS) was performed on bulk samples and on individual nanoparticles in high angle annular dark field (HAADF) – scanning transmission electron microscopy (STEM) mode. Compositions of approximately 55 particles were analyzed by EDS for each sample. Compositional distribution of elements in the random Pt-Pd nanoalloy sample is shown in Fig. 2. More details of the TEM analysis, including the aberration-corrected HAADF-STEM images of Pt@Pd, Pd@Pt, and the Pt-Pd nanoalloy, can be found in Ref. 25.

EXAFS experiments were performed at beamline X18B at the National Synchrotron Light Source (NSLS), Brookhaven National Laboratory, Upton, New York. The storage ring energy was 2.5 GeV and the ring current was in the range of 110–300 mA. A double-crystal Si (111) monochromator was used to scan x-ray energy from −150 eV to 1600 eV relative to the Pt L_3 edge (11 564 eV) and from −150 eV to 1500 eV relative to the Pd K edge (24 350 eV). In all cases the nanoparticle samples were dispersed in ethanol. The EXAFS data of the solutions were measured in transmission mode using custom-made sample holders. Standard metal (Pt and Pd) foils were placed between the transmission and reference x-ray detectors and measured simultaneously with all the nanoparticle samples for x-ray energy calibration and data alignment.

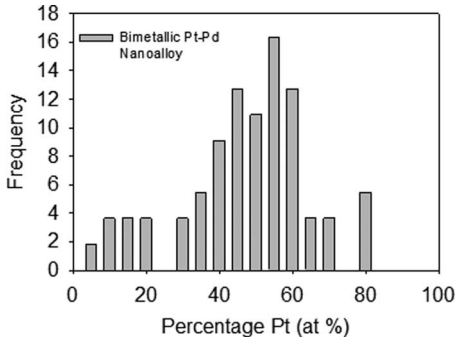

FIG. 2. Frequency distribution of Pt and Pd in Pt-Pd-alloy nanoparticle system measured by EDS in HAADF-STEM mode. The total of 55 particles were included in the distribution.

In EXAFS, information about the structural environment of the X-ray absorbing atom and its surroundings, including its dynamic changes, is extracted from the X-ray absorption coefficient $\mu(E)$ measured within 1000–1500 eV from the X-ray absorption edge energy. The oscillatory part of $\mu(E)$ results from the interference patterns of photoelectrons due to their scattering from neighboring atoms. It thus contains quantitative information about the local atomic environment in the proximity of the absorbing atom. The EXAFS signal $\chi(k)$ that originates from the nearest group of neighbors at approximately equal distances from the absorbing atoms (i.e., within the first shell) is often written as[28]

$$\chi(k) = \frac{S_0^2 N}{kR^2} |f^{\text{eff}}(k)| \sin[2kR + \delta(k)]\, e^{-2\sigma^2 k^2} e^{-2R/\lambda(k)}, \tag{2}$$

where k is the photoelectron wave number, $f^{\text{eff}}(k)$ and $\delta(k)$ are the photoelectron scattering-path amplitude and phase, respectively, S_0^2 is the passive electron reduction factor, N is the degeneracy of the scattering path (equal to the coordination number for the single-scattering paths), R is the effective half-path-length (which equals the interatomic distance for single-scattering paths), σ^2 is the mean-square deviation in R, also known as the second cumulant of the pair distribution function,[29] and $\lambda(k)$ is the photoelectron mean free path.

Data processing and analysis was performed using the IFEFFIT package.[30] The photoelectron scattering functions (amplitude and phase) for all first nearest neighbor (1NN) photoelectron paths were calculated using the FEFF6 program[28] and used to fit the EXAFS equation in r-space and derive the electronic (S_0^2, and the photoelectron energy origin correction, ΔE_0) and structural parameters (N, R, and σ^2) of the systems. The anharmonic correction was not included in the analysis presented because including it in the fit did not change the results within their experimental uncertainties.

In the bulk metal fits (Pt and Pd foils), the coordination number of the first nearest neighbor (1NN) bonds was fixed at 12 – the expected value for a face center cubic (fcc) lattice – and the S_0^2 parameters were varied. For the heterometallic systems, multiple-edge (Pd K and Pt L_3) analysis was done by fitting theoretical FEFF6 signals to their respective experimental data concurrently. The monometallic (Pd-Pd and Pt-Pt) paths were constructed using FEFF calculations done on the coordinates of the fcc Pd and Pt metal structures, respectively. To calculate FEFF theory for heterometallic paths (Pt-Pd and Pd-Pt), the opposite types of scattering atoms (a Pt scatterer for the Pd absorber and a Pd scatterer for the Pt absorber) were inserted into a 1NN position of the coordinate lists of the Pd and Pt atoms, respectively. In order to break the correlation between the amplitude factors in the fit, the S_0^2 parameters of the bimetallic systems were fixed to those obtained for bulk Pt and Pd (0.87 for both).

The fitting parameters were adjusted for both edge data concurrently, by applying several constraints in the analysis as follows. The bond lengths and mean squared bond length disorders of the Pt-Pd bond were constrained to be

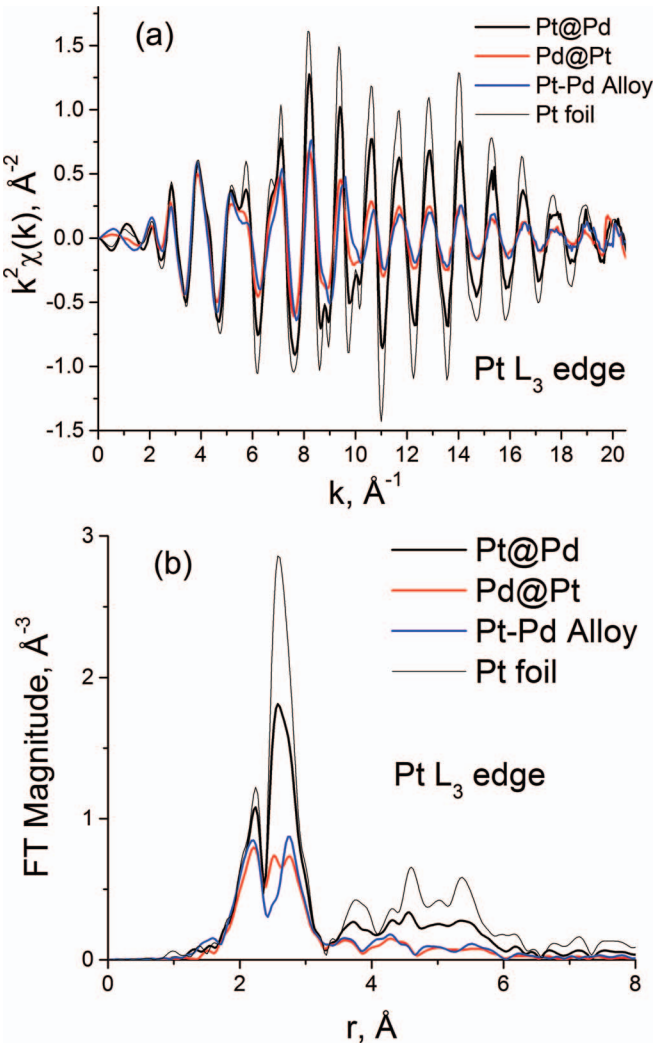

FIG. 3. k^2-weighted Pt L_3-edge EXAFS data (a) and their Fourier transform magnitudes (b) for the Pt bulk and the nanoparticle samples. The k-range in Fourier transforms was from 2 to 19 $Å^{-1}$.

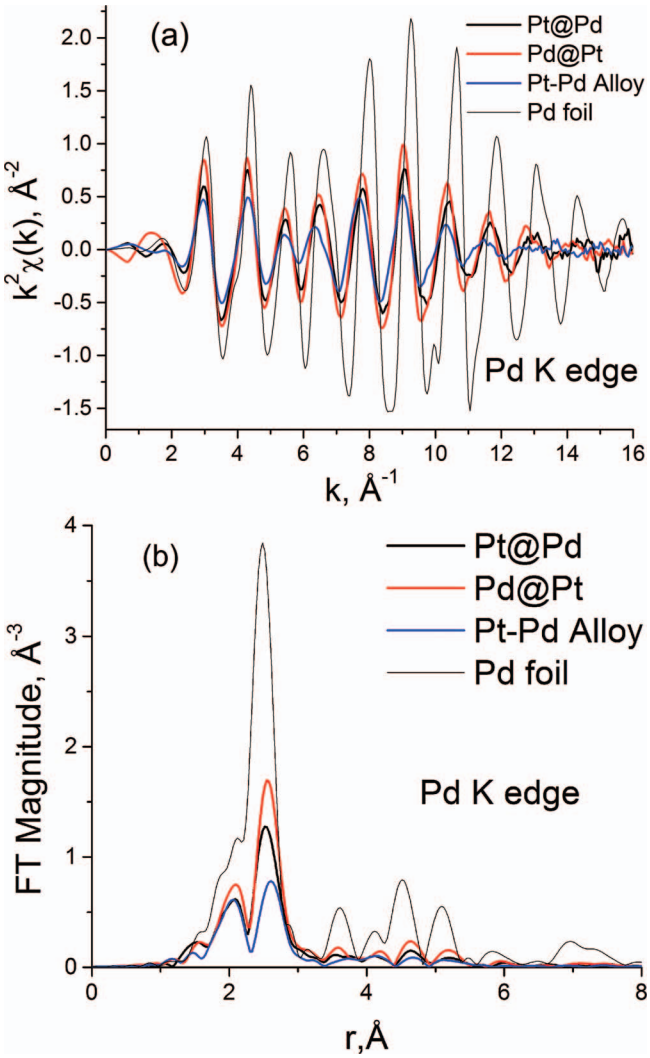

FIG. 4. k^2-weighted Pd K-edge EXAFS data (a) and their Fourier transform magnitudes (b) for the Pd bulk and the nanoparticle samples. The k-range in Fourier transforms was from 2 to 15 $Å^{-1}$.

the same as measured from either edge: $R_{\text{Pt–Pd}} = R_{\text{Pd-Pt}}$ and $\sigma^2_{\text{Pt–Pd}} = \sigma^2_{\text{Pd–Pt}}$. The coordination numbers were all varied independently, including those of the heterometallic (Pt-Pd and Pd-Pt) bonds. As a result, the bimetallic compositions x_{Pt} and x_{Pd} could be measured independently from the bulk,[16]

$$x_{\text{Pt}}/x_{\text{Pd}} = N_{\text{Pd–Pt}}/N_{\text{Pt–Pd}}. \quad (3)$$

The following parameters were varied in the EXAFS analysis: the corrections to the photoelectron energy origin (unique for each edge, hence the total of 2 variables), the 1NN coordination numbers (4 variables), the nearest neighbor bond lengths (3 variables), and the values of σ^2 (3 variables). In the case of Pt@Pd sample, we found it necessary to add Pd-O contributions to describe low r features in the Pd K-edge data. Therefore, three more variables (Pd-O coordination number, distance correction, and the disorder parameter) were included in that fit. The total number of relevant independent data points[31] was between 32 and 38, depending on the sample, i.e., much greater than the total number of variables (12–15).

IV. RESULTS AND DISCUSSION

Figures 3 and 4 present the raw k-space and r-space data for all of the samples. From visual examination of the Fourier transforms (Figs. 3(b) and 4(b)) we conclude that the atomic environments around Pt in the core (Figure 3(b)) and Pd in the core (Fig. 4(b)) resemble that of the bulk fcc structure of Pt and Pd, respectively. That observation is consistent with Pt segregating into a Pt-rich phase in the Pt@Pd sample, and Pd doing likewise in the Pd@Pt sample. It is expected that Pd EXAFS in Pt@Pd sample and Pt EXAFS in Pd@Pt sample should also resemble bulk Pd and Pt EXAFS data, respectively. Indeed, if 50% of all atoms are Pt and 50% are Pd, and if the majority of all Pt atoms are in the core, then the majority of Pd atoms must be on the surface. However, the effect of segregation on the ordering in bimetallic particles is very different from that in bulk alloys. In the latter, macroscopically segregated Pt-rich and Pd-rich regions would have corresponding EXAFS signals that would indeed resemble bulk Pt and Pd, respectively. In contrast, due to surface tension, the surface layers for nanoscale particles universally

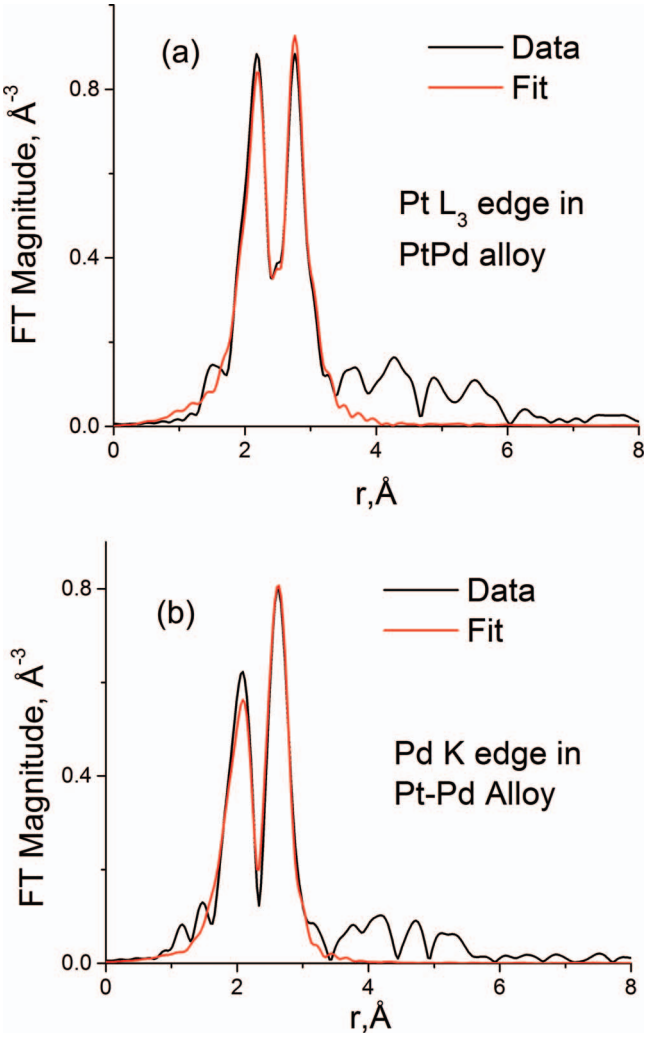

FIG. 5. Fourier transform magnitudes of the k^2-weighted data (black) and fit (red) of the Pt L_3-edge (a) and Pd K-edge (b) in the Pt-Pd nanoalloy samples. The k-ranges for Fourier transforms were from 2.5 to 17 $Å^{-1}$ and from 2 to 16.3 $Å^{-1}$, respectively. The fitting ranges were from 1.6 to 3.4 Å and from 1.2 to 3.4 Å, respectively.

exhibit disorder.[32] Hence, the EXAFS signal from those surface atoms is damped greater than that from the same atomic species when they are located in the core. Another factor that alters the EXAFS amplitude of the surface atoms compared to the same atomic species located in the core is the coordination number. Since the thickness of a spherical shell is smaller than the thickness of a spherical core of the same volume (as required in case of perfect core-shell segregation and 50-50 composition), it is expected that the atoms that are segregated to the surface have fewer neighbors of the same kind (and the total number of neighbors, for that matter) than those in the core. Hence, the EXAFS signal of those surface species is expected to be different from their respective bulk form, but whether the disorder or the surface truncation affects the data the most will be understood only during the data analysis.

Figure 5 presents the data and theoretical fits for the alloy nanoparticle system. For all systems studied, the fitting results for the 1NN coordination numbers, bond lengths, and their disorders are reported in Tables I–III, respectively. As discussed above, the Pt-Pt coordination numbers in Pt shell are lower than those in the Pt core, which is consistent with the atoms in the shell having a lower average coordination. The same observation is valid for the Pd-Pd coordination numbers (Table I). Of all the samples, only the Pd@Pt exhibits a strong disordering of the Pt-Pt bonds (Table III). However, a similar statement cannot be unambiguously stated for Pd in any of the structures due to the overlapping errors in the disorder parameters.

TABLE I. First nearest neighbor coordination numbers. Uncertainties in the last digits are in parentheses.

	$N_{\text{Pt-Pt}}$	$N_{\text{Pt-Pd}}$	$N_{\text{Pd-Pt}}$	$N_{\text{Pd-Pd}}$
Pt@Pd	9.8(4)	1.0(2)	2.1(4)	6.6(4)
Pd@Pt	7.9(6)	1.3(3)	2.7(7)	7.9(6)
Pt-Pd alloy	6.3(4)	2.6(3)	3.7(5)	3.2(5)

We now turn to the EXAFS-determined composition and compare it with that obtained independently by EDS. Table IV demonstrates that the Pt to Pd molar ratio in all bimetallic samples calculated using Eq. (3) results in an overestimate of the composition relative to the ratio measured by EDS. We attribute this discrepancy to the artifacts of EXAFS data analysis that can be due to one or more factors. These artifacts may arise from either a large disorder in one group of atomic species relative to another, or due to the role played by inter-cluster compositional polydispersity. For example, the Pd bonding environment is more disordered than that of Pt (Table IV). Strong disorder in Pd-rich regions (either core or shell) is likely to signal a greater asymmetry in both the Pd-Pt and Pd-Pd pair distribution functions. Consequently, the asymmetric disorder off the bonding leads to an underestimation of the number of Pd atoms within a given distance being probed at both the Pd and Pt edges.[33] Another possibility is that the effect of compositional polydispersity plays a role in this apparent discrepancy, as described in greater detail below.

The values of the total coordination numbers $N_{\text{Pt-}M}$ and $N_{\text{Pd-}M}$, and the short range order parameters α for the Pt-Pd and Pd-Pt first coordination spheres are reported in Table IV. The large positive values of α for the Pt@Pd and Pd@Pt system for the core element (Pt or Pd) indicate that these systems are heterogeneous, with locally Pt-rich and Pd-rich regions, as expected. As mentioned above, it is not possible to discriminate between intra-particle or inter-particle segregation using EXAFS alone. To make such a determination, additional intra-particle composition measurements were employed using a local method such as EDS. Figure 2 demonstrates that the alloy particles are bimetallic. As described above, the difference between the $N_{\text{Pt-}M}$ and $N_{\text{Pd-}M}$ values can be used to detect if/which species segregate to the core, and to the shell,

TABLE II. First nearest neighbor distances. Uncertainties in the last digits are in parentheses.

	$R_{\text{Pt-Pt}}$ (Å)	$R_{\text{Pt-Pd}}$ (Å)	$R_{\text{Pd-Pd}}$ (Å)
Pt@Pd	2.757(1)	2.776(8)	2.776(3)
Pd@Pt	2.755(4)	2.758(11)	2.788(5)
Pt-Pd alloy	2.745(3)	2.751(5)	2.766(7)

TABLE III. First nearest neighbor disorder parameters. Uncertainties in the last digits are in parentheses.

	$\sigma^2_{\text{Pt-Pt}}$ (Å^2)	$\sigma^2_{\text{Pt-Pd}}$ (Å^2)	$\sigma^2_{\text{Pd-Pd}}$ (Å^2)
Pt@Pd	0.0055(1)	0.0070(12)	0.0080(4)
Pd@Pt	0.0074(4)	0.0077(16)	0.0081(6)
Pt-Pd alloy	0.0064(3)	0.0066(6)	0.0070(10)

of the bimetallic particle. As Table IV demonstrates, the $N_{\text{Pt-}M} > N_{\text{Pd-}M}$ in Pt@Pd and $N_{\text{Pt-}M} < N_{\text{Pd-}M}$ in Pd@Pt, confirming the intended architecture of these core-shell systems.

These results demonstrate that knowledge of coordination numbers in heterometallic nanoparticles can reveal detailed insights into their compositional habits including the degree of short range order. The short range order, in turn, is a useful characteristic that communicates on the homogeneity or heterogeneity of alloying without needing to be verified *via* an independent method. Indeed, the large positive values of α present unambiguous evidence that Pt and Pd atoms are not homogeneously mixed in the Pt@Pd and Pd@Pt samples.

The situation with the third sample, the nominally random Pt-Pd alloy, is more complicated. At first glance the small, but positive α value in Table IV would seem to indicate a tendency towards segregation. Such was the case, for example, of the segregation, demonstrated by EXAFS, in Pt-Ru[34] and Ir-Pt[35] bimetallic nanoparticles. In these examples, the particles had narrow compositional distributions (with standard deviations, measured by EDS, of 5%–10%) and could be visualized in terms of a "representative" heterogeneous bimetalic nanoparticle. However, when inter-particle variation in the composition is not negligible, the experimentally determined coordination numbers (i.e., found by EXAFS which is an ensemble-average method) will be incorrectly interpreted. We have recently shown[36] that alloys with broad compositional distributions are expected to have positive values for the ensemble-average short range order despite having a random intra-particle distribution of atoms. Hence, a random nanoalloy may be mistaken as a system with a core-shell motif if the NPs are not all stoichiometrically uniform.

This prediction can be illustrated by the following simple example. Assume that the sample consists of two groups of bimetallic nanoparticles. The first group consists of N particles where 30% of all atoms are A-type and 70% - B-type in each. The second group consists of N particles of 70% and 30% of A and B-type atoms, respectively. The average composition over the entire sample is then 50% of A and 50% of B atoms. Assume also that the distribution of atoms in each particle is random, i.e., the value of α calculated over each population is zero. Finally, assume that the geometry of all particles is the same and atoms occupy regular lattice sites. Ensemble-average calculation of the coordination numbers of AB type yields the following result: $N_{AB} = 0.3 \times 0.7N_{AM} + 0.7 \times 0.3N_{AM} = 0.42N_{AM}$. Hence, the ensemble-average value of α measured by EXAFS will be equal to 0.16 (Eq. (1)), in apparent contradiction to the local randomness ($\alpha = 0$) of each population. More general demonstration of this effect is presented in Refs. 7 and 36.

In the present case, the compositional distribution of atoms in the Pt-Pd alloy system is very broad (Fig. 2), with standard deviation of 18%. According to Ref. 36, the increase in σ_c causes the apparent coordination number of N_{AA} to increase and N_{AB} to decrease relative to their ideal values in a random distribution of A and B atoms. Estimates predict that standard deviation in compositional distribution of the order of 15% may cause the error of ca. 15%–20% in coordination numbers, causing the apparent N_{AA} to increase and N_{AB} to decrease relative to a "representative" nanoparticle at the average composition[36] This will be true for any particles that have the same size and average composition. Since the apparent N_{AB} decreases, the calculated value of α_{AB} will increase (Eq. (1)) and becomes positive, as in the example described above. Qualitatively, therefore, the experimentally measured standard deviation of 18% in the case of Pt-Pd alloy NPs should cause the *apparent* short range order parameter to be of the order of 20%, i.e., similar to its values obtained experimentally (Table IV). As discussed, it is merely an artifact of the ensemble averaging of EXAFS technique, and the conclusion to be made from this exercise is that the individual particles are likely to have zero short range order, or be characterized as random alloys.

V. SUMMARY AND CONCLUSIONS

In summary, we presented several criteria of homogeneity and short range order of nanoalloys that employ Cowley short range order parameters α. These parameters can be easily obtained by EXAFS analysis of partial coordination numbers. We demonstrated that the range of possible values of α for homogeneous systems is limited to $[\alpha_{\text{min}}, 0]$, where $-1 < \alpha_{\text{min}} < 0$. Within that range of α values, the alloys have short range order that vanishes for $\alpha = 0$ corresponding to a random alloy. For all other values of α the alloys are heterogeneous. We demonstrated also that the small positive values of α should be interpreted with extreme care. Namely, when the short range order parameter values are relatively small (less than ca. 20%–30%) it is required to examine the compositional distribution which was shown to bias EXAFS coordination numbers towards a tendency to segregation. For broad compositional distributions, such small positive values of α

TABLE IV. Bimetallic compositions obtained by EDS and EXAFS, total coordination numbers, and short range order parameters α. Uncertainties in the last digits are in parentheses.

	$x_{\text{Pt}}/x_{\text{Pd}}$ (EDS)	$x_{\text{Pt}}/x_{\text{Pd}}$ (EXAFS)	$N_{\text{Pt-}M}$ vs $N_{\text{Pd-}M}$	$\alpha_{\text{Pt-Pd}}$	$\alpha_{\text{Pd-Pt}}$
Pt@Pd	0.96 (Ref. 25)	2.1 ± 0.6	10.8(5) > 8.7(6)	+0.70	+0.66
Pd@Pt	0.89 (Ref. 25)	2.1 ± 0.7	9.2(7) < 10.6(9)	+0.53	+0.64
Pt-Pd alloy	0.82 (Ref. 25)	1.4 ± 0.3	8.9(5) > 6.9(7)	+0.27	+0.11

can be still consistent with homogeneous random alloys. Our work does not only uncover possible experimental artifacts but offers corrective strategies. In the case of broad compositional distributions, their measurement by a local method such as EDS can be used to retrieve the short range order parameters in sub-sets of individual nanoparticles.

ACKNOWLEDGMENTS

We acknowledge the support of this work by the (U.S.) Department of Energy (DOE) Grant No. DE-FG02-03ER15476. X18B beamline is supported, in part, by Synchrotron Catalysis Consortium (DOE Grant No. DE-FG02-05ER15688).

[1]A. Roucoux, J. Schulz, and H. Patin, Chem. Rev. **102**, 3757–3778 (2002).
[2]B. Lim, M. Jiang, P. H. C. Camargo, E. C. Cho, J. Tao, X. Lu, Y. Zhu, and Y. Xia, Science **324**, 1302–1305 (2009).
[3]D. W. Elliott and W.-X. Zhang, Environ. Sci. Technol. **35**, 4922–4926 (2001).
[4]F. Tao, M. E. Grass, Y. Zhang, D. R. Butcher, J. R. Renzas, Z. Liu, J. Y. Chung, B. S. Mun, M. Salmeron, and G. A. Somorjai, Science **322**, 932–934 (2008).
[5]F. He and D. Zhao, Environ. Sci. Technol. **39**, 3314–3320 (2005).
[6]J. Greeley, T. F. Jaramillo, J. Bonde, I. B. Chorkendorff, and J. K. Norskov, Nat. Mater. **5**, 909–913 (2006).
[7]A. I. Frenkel, Chem. Soc. Rev. **41**, 8163–8178 (2012).
[8]Y. Xia, Y. Xiong, B. Lim, and S. E. Skrabalak, Angew. Chem., Int. Ed. **48**, 60–103 (2009).
[9]B. Wiley, Y. Sun, and Y. Xia, Acc. Chem. Res. **40**, 1067–1076 (2007).
[10]C. J. Murphy, T. K. Sau, A. M. Gole, C. J. Orendorff, J. Gao, L. Gou, S. E. Hunyadi, and T. Li, J. Phys. Chem. B **109**, 13857–13870 (2005).
[11]N. R. Jana, L. Gearheart, and C. J. Murphy, Adv. Mater. **13**, 1389–1393 (2001).
[12]J. K. Norskov, T. Bligaard, J. Rossmeisl, and C. H. Christensen, Nat. Chem. **1**, 37–46 (2009).
[13]B. Hammer and J. K. Norskov, Adv. Catal. **45**, 71–129 (2000).
[14]B. Hammer, Top. Catal. **37**, 3–16 (2006).
[15]R. V. Chepulskii and S. Curtarolo, ACS Nano **5**, 247–254 (2011).
[16]A. Frenkel, Z. Kristallogr. **222**(11), 605–611 (2007).
[17]B. J. Hwang, L. S. Sarma, J. M. Chen, C. H. Chen, S. C. Shih, G. R. Wang, D. G. Liu, J. F. Lee, and M. T. Tang, J. Am. Chem. Soc. **127**(31), 11140–11145 (2005).
[18]A. M. Beale and B. M. Weckhuysen, Phys. Chem. Chem. Phys. **12**(21), 5562–5574 (2010).
[19]U. D. Kulkarni, S. Banerjee, and R. Krishnan, Mater. Sci. Forum **3**, 111–121 (1985).
[20]E. Ma, Prog. Mater. Sci. **50**, 413–509 (2005).
[21]J. M. Cowley, Phys. Rev. **77**, 669–675 (1950).
[22]J. M. Cowley, Phys. Rev. **120**, 1648–1657 (1960).
[23]J. M. Cowley, Phys. Rev. **138**(5A), A1384–A1389 (1965).
[24]A. I. Frenkel, V. S. Machavariani, A. Rubshtein, Y. Rosenberg, A. V. Voronel, and E. A. Stern, Phys Rev B **62**, 9364 (2000).
[25]S. I. Sanchez, M. W. Small, J.-M. Zuo, and R. G. Nuzzo, J. Am. Chem. Soc. **131**(24), 8683–8689 (2009).
[26]J. Yang, J. Y. Lee, Q. Zhang, W. Zhou, and Z. Liu, J. Electrochem. Soc. **155**(7), B776–B781 (2008).
[27]Y. Wang and N. Toshima, J. Phys. Chem. B **101**(27), 5301–5306 (1997).
[28]S. I. Zabinsky, J. J. Rehr, A. Ankudinov, R. C. Albers, and M. J. Eller, Phys. Rev. B **52**(4), 2995–3009 (1995).
[29]G. Bunker, Nucl. Instrum. Methods **207**, 437–444 (1983).
[30]M. Newville, J. Synchrotron Radiat. **8**, 322 (2001).
[31]E. A. Stern, Phys. Rev. B **48**, 9825–9827 (1993).
[32]J. S. Vermaak, C. W. Mays, and D. Kuhlmann, Surf. Sci. **12**(2), 128–133 (1968).
[33]A. Yevick and A. I. Frenkel, Phys. Rev. B **81**(11), 115451 (2010).
[34]M. S. Nashner, A. I. Frenkel, D. L. Adler, J. R. Shapley, and R. G. Nuzzo, J. Am. Chem. Soc. **119**(33), 7760–7771 (1997).
[35]M. W. Small, S. I. Sanchez, L. D. Menard, J. H. Kang, A. I. Frenkel, and R. G. Nuzzo, J. Am. Chem. Soc. **133**(10), 3582–3591 (2011).
[36]A. I. Frenkel, A. Yevick, C. Cooper, and R. Vasic, Ann. Rev. Anal. Chem. **4**, 23–39 (2011).